

## MIT Open Access Articles

### *Precision spectroscopy of fast, hot, exotic isotopes using machine-learning-assisted event-by-event Doppler correction*

The MIT Faculty has made this article openly available. **Please share** how this access benefits you. Your story matters.

**Citation:** Udrescu, S. M., Torres, D. A. and Garcia Ruiz, R. F. 2024. "Precision spectroscopy of fast, hot, exotic isotopes using machine-learning-assisted event-by-event Doppler correction." *Physical Review Research*, 6 (1).

**As Published:** 10.1103/physrevresearch.6.013128

**Publisher:** American Physical Society

**Persistent URL:** <https://hdl.handle.net/1721.1/153541>

**Version:** Final published version: final published article, as it appeared in a journal, conference proceedings, or other formally published context

**Terms of use:** Creative Commons Attribution




## Precision spectroscopy of fast, hot, exotic isotopes using machine-learning-assisted event-by-event Doppler correction

S. M. Udrescu <sup>1,\*</sup>, D. A. Torres <sup>2</sup> and R. F. Garcia Ruiz <sup>1</sup>

<sup>1</sup>*Massachusetts Institute of Technology, Cambridge, Massachusetts 02139, USA*

<sup>2</sup>*Departamento de Física, Universidad Nacional de Colombia, Bogotá 111321, Colombia*

 (Received 23 April 2023; revised 21 November 2023; accepted 21 December 2023; published 31 January 2024)

We propose an experimental scheme for performing sensitive, high-precision laser spectroscopy studies on fast exotic isotopes. By inducing a stepwise resonant ionization of the atoms traveling inside an electric field and subsequently detecting the ion and the corresponding electron, time-, and position-sensitive measurements of the resulting particles can be performed. Using a mixture density network, we can leverage this information to predict the initial energy of individual atoms and thus apply a Doppler correction of the observed transition frequencies on an event-by-event basis. We conduct numerical simulations of the proposed experimental scheme and show that kHz-level uncertainties can be achieved for ion beams produced at extreme temperatures ( $>10^8$  K), with energy spreads as large as 10 keV and nonuniform velocity distributions. The ability to perform in-flight spectroscopy, directly on highly energetic beams, offers unique opportunities to study short-lived isotopes with lifetimes in the millisecond range and below, produced in low quantities, in hot and highly contaminated environments, without the need for cooling techniques. Such species are of marked interest for nuclear structure, astrophysics, and new physics searches.

DOI: [10.1103/PhysRevResearch.6.013128](https://doi.org/10.1103/PhysRevResearch.6.013128)

### I. INTRODUCTION

With the advent of new radioactive beam facilities worldwide, short-lived nuclei that hitherto have only existed in stellar explosions are being created artificially in the laboratory, extending our exploration of the nuclear chart to extreme proton-to-neutron ratios [1–3]. These unstable isotopes, typically with lifetimes of just a fraction of a second, are critical for our fundamental understanding of nuclei and nuclear matter [2]. The major challenge of current experimental nuclear physics is to develop sensitive and precise techniques to enable the study of these exotic isotopes, commonly produced at high temperature and with yields of just a few isotopes per second [1–3].

Laser spectroscopy has long been established as an important tool for studying the properties of unstable nuclei [2]. This technique allows the extraction of nuclear spins, electromagnetic moments, and changes in the nuclear root-mean-square charge radii [2,3]. These observables are key for understanding the atomic nucleus and guiding developments of nuclear theory [4–10]. To extract nuclear properties from atomic spectra, high experimental sensitivity and precision are critical. Laser cooling and trapping techniques represent some of the most precise experimental methods [11,12], but they

are not universally applicable to all elements of the periodic table and cannot be employed directly to study short-lived nuclei, typically produced at high temperatures, high energies ( $>30$  keV), and with subsecond lifetimes [2].

A highly successful approach to overcome these challenges is the collinear laser spectroscopy technique applied on bunched ion beams [13]. Unstable isotopes, typically produced from nuclear reactions, can be mass separated as ions, trapped, and then cooled in gas-filled radio-frequency ion traps [13,14]. Buffer gas collisions are then used to reduce the temperature of the initial beam down to the temperature of the gas. These methods have allowed high-precision measurements of a wide range of radioactive nuclei [2] and have recently been extended to study radioactive molecules [15–18]. However, the lifetime of the systems that can be studied with such experiments is limited by the cooling and trapping time, which are typically on the order of tens or hundreds of milliseconds [13]. Moreover, trapping becomes impractical when large amounts of contaminants are present, overfilling the trap, and preventing the capture of the ion of interest. New-generation radioactive beam facilities, such as the Facility for Rare Isotopes Beams (FRIB) [19] in the U.S. and RIKEN in Japan [20], are already producing isotopes at the extreme of stability, but due to their short lifetimes ( $<5$  ms) they cannot be studied with the current laser spectroscopy techniques. Therefore, spectroscopy methods that could be directly applied to fast, hot, short-lived isotopes need to be developed [21,22].

Here, we propose a simple, versatile method for performing high-precision laser spectroscopy studies of fast atomic beams in a way that allows the energy of the atoms of interest to be measured in flight on an event-by-event basis.

\*sudrescu@mit.edu

*Published by the American Physical Society under the terms of the Creative Commons Attribution 4.0 International license. Further distribution of this work must maintain attribution to the author(s) and the published article's title, journal citation, and DOI.*

By performing coincidence measurements of the resonant ions and ejected electrons produced during a resonant laser ionization process, the vector velocity of each initial atom can be reconstructed, enabling accurate measurements of the transitions of interest. This setup would enable precision laser spectroscopy measurements directly on isotopes produced by in-flight reactions, with energy spreads as large as 10 keV and lifetimes below one millisecond or on ions produced after molecular breakup reactions. We demonstrate that precision measurements can be achieved even for arbitrary energy distributions of the initial particles, without the need for cooling mechanisms.

To highlight the broad applicability of our proposed method, we present three different physics scenarios:

(i) *Atomic spectroscopy of Sn isotopes.* Sn is the element with the largest number of stable isotopes (ten). Precision isotope shift measurements over this long isotope chain could provide complementary studies to constrain the possible existence of new fundamental forces and particles [23]. Having a proton magic number,  $Z = 50$ , Sn isotopes possess a relatively simple nuclear structure and thus exhibit reduced sensitivity to Standard Model effects, such as nuclear deformation [23,24], facilitating a clear identification of any new physics signals.

(ii) *Charge radii measurement of Boron isotopes.* Located along the proton drip-line, the  ${}^8\text{B}$  isotope is of particular interest for nuclear structure studies, being a main candidate for displaying a proton halo [25–28]. This behavior would manifest as an increased value of the charge radius of  ${}^8\text{B}$ , which can be extracted, in a model independent way, through isotope shifts measurements.  ${}^8\text{B}$  is also of interest for solar neutrino physics [29,30]. Its production in the sun, through the proton capture on a  ${}^7\text{Be}$  nucleus, is accompanied by a high-energy neutrino emission [26,29]. The rate of this process depends on the structure of the  ${}^8\text{B}$  nucleus [26,29,30]. Despite having a relatively long lifetime ( $\tau = 770$  ms) its spectroscopic investigation has not been possible so far, mainly due to its high reactivity in forming molecules, and the low efficiency of deceleration and trapping for elements with small mass [28].

(iii) *Charge radii measurements of Ni isotopes at the extreme of stability.* With both neutron and proton magic numbers at  $N = 20$  and  $Z = 28$ , respectively,  ${}^{48}\text{Ni}$  is of marked interest for nuclear structure and the study of exotic nuclear phenomena at the edge of stability [31,32]. Although this isotope can be produced at the current radioactive beam facilities, its short lifetime ( $\tau = 2.1$  ms) prevents its study using available laser spectroscopy techniques.  ${}^{48}\text{Ni}$  is the mirror nucleus of the stable doubly magic  ${}^{48}\text{Ca}$ , hence a measurement of the nuclear charge radii difference between these two isotopes can be highly sensitive to constrain parameters of the equation of state of nuclear matter [33].

## II. EXPERIMENTAL APPROACH

A schematic of our proposed method is shown in Fig. 1. An ion beam, whose energy and energy spread depend on the isotopic production mechanism, is neutralized in-flight and then sent towards the experimental interaction region. There, after the non-neutralized ions are removed, the remaining atoms are overlapped collinearly with a continuous-wave

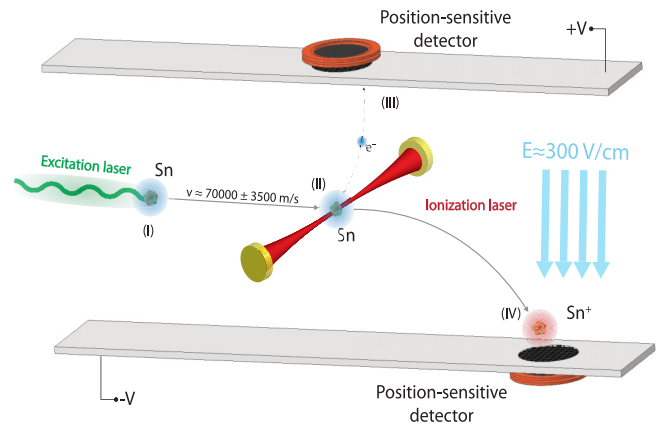


FIG. 1. Illustration of the experimental setup. The neutral atoms resulting from the neutralization process (not shown) enter the interaction region where they are excited to a higher-lying electronic state by a collinear laser (I). The excited atoms are then ionized by a standing-wave laser inside an optical cavity (II). The resulting electrons are detected by a position-sensitive detector located above the ionization point (III), while the ions continue their trajectories in the electric field produced in between two parallel plates, until they reach a second position-sensitive detector (IV). The direction and magnitude of the electric field experienced by the ions is shown in light blue.

laser, such that they are resonantly excited to a particular electronic state. The laser power and beam diameter will depend on the properties of the atomic beam under investigation, such as its spatial and energy spread. After this, the atoms can be ionized by a different continuous-wave laser beam, perpendicular to the atoms' propagation direction. As this second step can be a non-resonant process, power densities on the order of tens to thousands of  $\text{kW}/\text{cm}^2$  can be required for efficient (50% – 100%) ionization [34]. This can be achieved by using a standing-wave laser built inside an optical cavity [35]. Similar to the excitation step case, the ionization laser beam diameter will depend on the properties of the atomic beam. We expect that a diameter of a few mm [35] will be suitable for an effective ionization. Below we briefly describe possible experimental implementations for the study of the considered isotopes:

(i) Singly charged  ${}^{120}\text{Sn}$  ions can be produced by laser ablation at relatively low energies in large amounts ( $> 10^9$  ions/s). This element can be neutralized with high efficiency by collisions with alkali metals [36,37]. To highlight the ability of our proposed method to perform precision experiments on ion beams of large energy spread, we assume an initial energy of  $10 \pm 1$  keV.

(ii)  ${}^8\text{B}$  isotopes can be produced by impinging a  ${}^6\text{Li}$  beam on a  ${}^3\text{He}$  target [38]. After passing through a gas catcher, significantly reducing their energies,  ${}^8\text{B}$  emerges mainly as molecular ions, which then enter an radio frequency quadrupole cooler and buncher [28]. From here, the molecular ions can be sent towards the interaction region with an energy on the order of tens of keV, a cross section of a few mm, and an energy spread of  $< 1$  eV [14,28,39–41]. The molecular ions can be passed through a nanometer-thin carbon foil [28] to cause molecular breakup and produce the desired atoms of

$^8\text{B}$ . The energy of the resulting beam, as well as its charge state, depends on the initial energy of the molecular ions as well as the thickness of the carbon foil [28,42]. For an output energy on the order of 1 keV, 90% of the output beam can contain neutral boron [28,42]. In our setup, such a carbon foil can be placed a few centimeters in front of the interaction region with ionization laser. This ensures that the optical cavity performance is not affected (the radius of the laser beam inside the ionization cavity is expected to be  $<5$  mm) and that the resulting  $^8\text{B}$  ions are deflected from the neutral beam. The energy spread of the  $^8\text{B}$  atoms is expected to be on the order of the molecular dissociation energy, which can be in the range of 1 to few tens of eV [43]. Here, we assume a conservative value of 100 eV energy spread for the  $^8\text{B}$  atomic beam, ending up with a total energy of  $1000 \pm 100$  eV. Given the proximity of the carbon foil to the ionization point, as well as the higher longitudinal (along the beamline axis) energy ( $\sim 1000$  eV), relative to the transverse energy ( $<100$  eV), the spatial spread of the ions is expected to be on the order of one centimeter, thus most of the ions can be overlapped with the laser beams. Assuming an excitation laser linewidth of 100 MHz [34], an overall efficiency of  $\sim 0.1\%$  can be expected [2], defined as the number of  $^8\text{B}$  ions detected in coincidence with their respective electron after ionization, over the number of atoms produced after the interaction with the carbon foil.

(iii)  $^{48}\text{Ni}$  isotopes can be produced by in-flight nuclear reactions with energies on the order of hundreds of MeV/u [19,20,44]. This can be reduced down to  $\sim 1$  MeV by collisions with solid targets [44]. The transverse diameter of the beam at this stage is expected to be on the order of a few centimeters [45]. From here, we assume the ion beam can be decelerated to 100 keV. To maximize the transmission efficiency during the deceleration step, a custom deceleration setup needs to be implemented, which will strongly depend on the initial beam properties and thus requires a detailed experimental investigation for each specific experimental setup. The energy spread of the beam also depends on the deceleration stages. For the analysis below, we assume an energy spread of 10% of the total beam energy, leading to a final value for the energy of the  $^{48}\text{Ni}$  beam to be  $100 \pm 10$  keV. The produced ions can be highly charged, thus they need to be neutralized by collisions with a gas [36] or solid targets [46–48], which can lead to species with  $+1$  or  $0$  charge states on nanoseconds timescales [46–48]. The optimal neutralization setup as well as its efficiency will depend on the properties of the initial ion beam. Assuming a 100 MHz linewidth for the first step laser [34], we expect, given the energy and energy spread considered, an excitation efficiency of  $10^{-3}$ . A further reduction in efficiency of about two orders of magnitude is expected from the laser-atom overlap, assuming a diameter of the atomic beam on the order of a few centimeters [45], which is a factor of 10 larger than the expected laser beam diameter. Finally, based on particle trajectory simulations, we expect a transmission efficiency higher than  $\sim 0.1\%$  to the interaction region during the deceleration process to 100 keV. Hence, the total experimental efficiency, defined as the ratio of the number of ions detected in the interaction region in coincidence with an electron to the number of ions produced at  $\sim 1$  MeV, is estimated to be higher than  $10^{-8}$  for our proposed method.

It should be noted that the efficiency losses are dominated by the large energy spread and spatial dispersion introduced during the deceleration process. A detailed investigation of these effects is beyond the scope of our paper. For comparison with current techniques, at FRIB [19], the overall efficiency of decelerating and cooling  $^{48}\text{Ni}$  isotopes for laser spectroscopy experiments, such as the BECOLA facility [14], is expected to be less than  $10^{-15}$ , seven orders of magnitude smaller than the lower limit expected from our proposed method.  $^{48}\text{Ni}$  is an extreme example, presented here as a pedagogical illustration to highlight the orders of magnitude in sensitivity gain that our proposed method can provide for short-lived isotopes at the very extreme of existence. Independent developments in efficient deceleration and beam transport should be addressed to be able to perform any laser spectroscopy measurement with this isotope. A realistic estimation of the expected rates of  $^{48}\text{Ni}$  requires an experimental characterization of beam properties and stopping efficiencies at the existing RIB facilities [19,20,44]. Below we investigate the energy reconstruction efficiency and resolution for  $^{48}\text{Ni}$  isotopes, assuming they are able to reach the interaction region.

The ionization step takes place within the electric field created between two parallel plates. The voltage between the plates, as well as their dimensions, will depend on the energy of the atomic beam. The frequency of the ionization laser can be selected to either directly ionize the atom to the continuum or to excite it to a Rydberg state, from where it can be ionized by the electric field. A position-sensitive detector, located right above the interaction region, can be used to detect individual electrons produced during the ionization process [49–51]. The region on the position sensitive detector where the electrons will be observed is expected to be of similar size to the diameter of the ionization laser beam. Thus, a position sensitive active area of  $\sim 10$  mm would be suitable. This will allow the extraction of the atom's initial position and time at the moment of the ionization. After that, the ion will move in the existing electric field until it reaches a second position-sensitive detector, such that the ion's final position and time of flight can also be recorded. The diameter of this position sensitive detector will depend on the energy spread of the beam and the voltage applied between the two electrode plates. The location of the two detectors can be chosen such that virtually all the produced electrons and ions are detected (up to the intrinsic efficiency of the detectors, which can be above 80% [52,53]). Using the initial and final position of the ions, as well as their time of flight, the initial ion velocity can be inferred as described below.

In the ideal case of a charged particle moving in an uniform field created by two parallel plates, one can analytically compute the particle trajectory and hence extract its initial velocity. In reality, different experimental uncertainties need to be accounted for, such as edge effects due to the finite size of the electrodes or uncertainties in the applied potentials and geometry of the experimental array. The effect of these uncertainties can be overcome by using a reference atom with a well-known electronic transition. To provide a realistic example,  $^{40}\text{Ca}$  and its  $^1S_0(4s^2) \rightarrow ^3P_1(4s4p)$  transition at 657 nm [54,55] can be used as a reference. For each ionization event, given the known frequency of the excitation step,  $\nu_{\text{laser}}$ , as well as the real frequency in the atom's rest-frame,  $\nu_{\text{atom}}$ , the



ion velocity,  $v$ , and thus energy,  $E$  can be extracted using the Doppler correction formula. The uncertainty on the measured energy for each event is given by  $dE = m_r v c (1 - \frac{v}{c}) \frac{dv_{\text{atom}}}{v_{\text{atom}}}$ , where  $dv_{\text{atom}}$  is the linewidth of the transition,  $m_r$  is the atom's mass, and  $c$  is the speed of light. The experiment will then be repeated with the atom of interest, labeled as the target atom, recording its initial and final position, time of flight, and the laser frequency measured during an ionization event.

For a system of nonrelativistic particles experiencing only electrostatic fields, two ions with different masses but the same charge state follow identical trajectories. Moreover, the time of flight between two given points is related simply by the square root of the mass ratios of the two species,  $R \equiv \sqrt{m_r/m_t}$ , where  $m_t$  is the mass of the target atom. Thus, the energy of the atom of interest can be obtained by comparing its time of flight, initial, and final positions with those of the reference atom. By predicting the energy of each individual target atom, while knowing the frequency of the laser used during an ionization event, the transition frequency in the atom's rest frame can be obtained on an event-by-event basis by using a neural network (NN).

As the parameter space of the two species is almost identical, NNs are ideally suited for the task, given their well-known power of interpolation. The main drawback of standard, feed-forward NN is that there is no statistically consistent way of estimating the uncertainties associated with the predicted values, which is critical for high-precision experiments. To overcome this challenge, a mixture density network (MDN) can be used [56]. Similar to regular NNs, MDNs take a vector as input, which in this case is  $\mathbf{x} = (x_i, x_f, t)$  for each individual ion, which is then passed through one or more hidden layers. However, unlike standard NNs, where the output is a deterministic function of the input, the output of an MDN is represented by a mixture of Gaussian functions:

$$\mathbf{y}(\mathbf{x}) = \sum_{i=1}^N \alpha_i(\mathbf{x}) \mathcal{N}(\mu_i(\mathbf{x}), \sigma_i(\mathbf{x})), \quad (1)$$

where  $\mu_i(\mathbf{x})$ ,  $\sigma_i(\mathbf{x})$  and  $\alpha_i(\mathbf{x})$  are functions learnt during the NN training, and  $N$  is the number of Gaussian components. In addition, the loss function of an MDN is a log-likelihood loss,

$$\mathcal{L} = -\ln \left( \sum_{i=1}^N \frac{\alpha_i(\mathbf{x})}{(2\pi)^{m/2} \sigma_i(\mathbf{x})} \exp \left[ -\frac{|\mathbf{E} - \mu(\mathbf{x})|^2}{2\sigma_i(\mathbf{x})^2} \right] \right), \quad (2)$$

where  $\mathbf{E}$  is the vector of energies of the training data. Thus, after training the network using the reference atom measurements, the energy value and the associated uncertainty can be predicted for each event measured for the atom of interest.

### III. RESULTS AND DISCUSSION

To illustrate the overarching capabilities of our approach, we have selected as the isotopes of interest:  $^{120}\text{Sn}$  with its transition  $^3P_0(5s^25p^2) \rightarrow ^1S_0(5s^25p^2)$  at 583 nm [23],  $^8\text{B}$  with its transition  $^2P_{1/2}(2s^22p) \rightarrow ^2S_{1/2}(2s^23s)$  at 250 nm [57], and  $^{48}\text{Ni}$  with the transition  $^3F_3(4s^2) \rightarrow ^5P_2(4s4p^2)$  at 255 nm [58], respectively. Precision isotope shift measurements for the isotopic chains of Sn, Ni, and B are of marked interest for nuclear structures [6,25–27,37,59,60], nuclear matter [33,61], astrophysics [29,30], and new physics

searches [23,62,63]. These elements have not been laser cooled yet, consequently, achieving precision measurements with the current laser spectroscopy techniques is particularly challenging.

Numerical simulations of electric fields and ion beam trajectories were performed using the software SIMION [64]. To prove our ability to properly reconstruct the correct rest frame transition frequencies of interest, the ions and electrons are produced in between the two parallel plates, just below a position-sensitive detector. The plates are rectangular, of dimensions 50 cm (along the atoms propagation direction)  $\times$  8 cm. The second position sensitive detector is assumed to have a diameter of 40 mm for the case of  $^{120}\text{Sn}$  and  $^8\text{B}$  and 60 mm for the case of  $^{48}\text{Ni}$  (a diameter of 10 mm is suitable for the first position sensitive detector in both cases). The distance between the position sensitive detectors is set to 20 cm for  $^{120}\text{Sn}$ , 11 cm for  $^8\text{B}$ , and 63 cm for  $^{48}\text{Ni}$ . These parameters allow virtually all the simulated ions to be detected. The ions' initial position is assumed to be distributed according to a 3D Gaussian with a standard deviation of 1 mm. This is a reasonable value given the laser beam diameters that can be achieved in high-power optical cavities [35]. The simulations were performed with a potential difference between the two plates, located 20 cm apart, of 6 kV for  $^8\text{B}$  and 20 kV for  $^{120}\text{Sn}$  and  $^{48}\text{Ni}$ . The electrons are assumed to be produced with nearly zero kinetic energy, which can be achieved by setting the ionization laser close to the IP of the atom or by exciting the atom to a Rydberg state and then performing field ionization. The time-of-flight of the electrons was calculated, resulting in a distribution with a standard deviation of less than 30 ps, which is below the resolution of typical position-sensitive detectors (which we assume in this paper to be 50 ps [52,53]). This uncertainty was added in quadrature to the time-of-flight uncertainty due to detectors' resolution,  $dt$ . The uncertainties on the initial,  $dx_i$  and final,  $dx_f$  position are given by the detector's resolution, which is assumed to be 10  $\mu\text{m}$ . For the reference atom, for each event, a Gaussian noise of mean zero and standard deviation given by the above-mentioned uncertainties ( $dx_i$ ,  $dx_f$ ,  $dt$ ,  $dE$ ) was added to the values of the initial and final position, time of flight, and initial ion energy, which are then recorded. The same steps were followed for the target atom, except that the initial energy information was assumed to be unknown.

For our numerical simulations, for each of the two considered cases,  $2 \times 10^8$  ions were generated, corresponding to the reference atom. Half of them were used for training and the other half for validation, allowing us to optimize the hyperparameters of the MDN. The MDN used in this work was implemented in PyTorch [65] and its architecture is shown in Fig. 2. It had one hidden layer of ten nodes and one Gaussian component. This allowed us to achieve the desired level of prediction accuracy, without using a large number of model parameters and thus avoid overfitting. The nonlinearity used for the hidden layer was an exponential linear unit (ELU) activation function, as suggested in Ref. [66], given by

$$\text{ELU}(x) \equiv \begin{cases} x & \text{if } x > 0 \\ e^x - 1 & \text{if } x \leq 0. \end{cases} \quad (3)$$

The MDN was trained for 6000 epochs with a starting learning rate of  $10^{-2}$ , which was reduced by a factor of 10

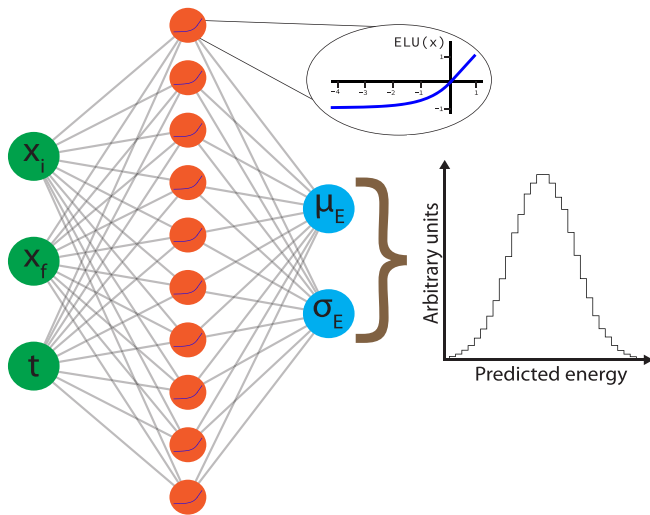


FIG. 2. Architecture of the employed MDN. The initial ( $x_i$ ) and final ( $x_f$ ) positions of the ions as well as their time of flight ( $t$ ) are used as inputs (green disks). They are passed to a hidden layer containing ten nodes (orange disks), each with an exponential linear unit (ELU) activation function, shown in the magnified view. For each input, the MDN predicts a mean and standard deviation for the energy distribution (blue disks), from which the energy of the event can be sampled.

every 1000 epochs. This learning schedule was chosen based on numerical experiments using the validation data, being suitable for achieving the prediction accuracy presented below. To further reduce the risk of overfitting, we used the Adam optimizer [67], which is a stochastic gradient descent method, with a batch size of 1024. Using the trained NN, we predicted the energy and associated rest frame transition frequency uncertainty for each event of the target atom. Figure 3 shows the obtained results. For the simulations involving  $^{120}\text{Sn}$ , Fig. 3(a) displays a histogram of the MDN's prediction error defined as  $E_{\text{pred}} - E_{\text{real}}$  in eV, having a standard deviation of 2.3 eV. This is a significant uncertainty reduction relative to the initial spread of 1000 eV. For  $^8\text{B}$ , the energy uncertainty is reduced from 100 eV to 0.4 eV [Fig. 3(c)], while for  $^{48}\text{Ni}$ , the energy uncertainty was reduced from 10 keV to only 77 eV [Fig. 3(e)]. In all three cases,  $\sim 95\%$  of the MDN's predictions are within two standard deviations from the true energy value, proving the reliability of the MDN's estimation of individual energies and associated uncertainties.

Using the predicted mean and standard deviation of the energy, as well as the laser frequency used when an event was observed, we can calculate the transition frequency in the rest frame of the target atom, together with its associated uncertainty on an event-by-event basis. In our simulation, this is done as follows. For each event, we sample the true rest-frame frequency using a Lorentzian distribution with mean and linewidth given by the transition of interest mentioned above. We Doppler shift it to the laboratory frame using the real energy of the ion, taken from SIMION, thus obtaining the laser frequency at which the given event was observed. Finally, we Doppler correct back to the ion's rest frame using the MDN predicted energy. The final value of the transition, obtained from  $N$  measured events, will be given

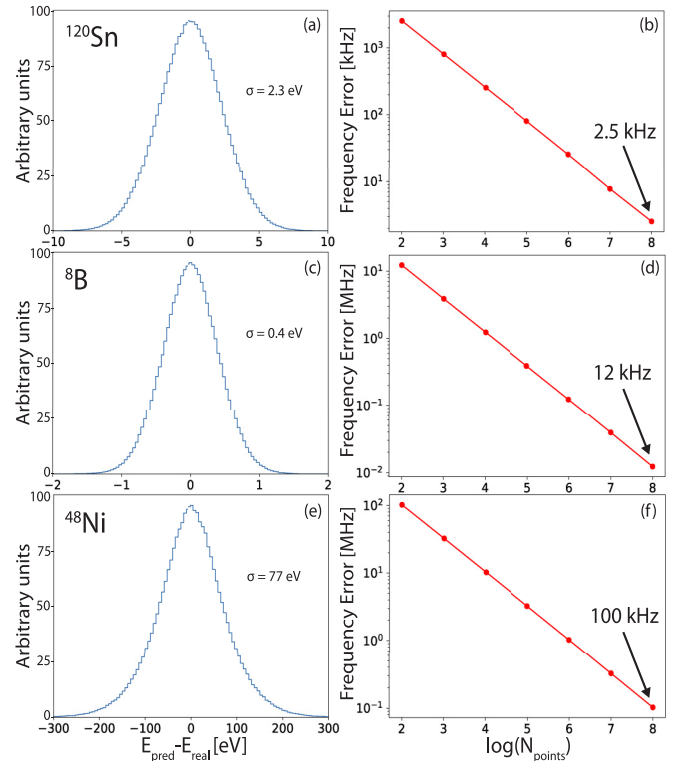


FIG. 3. Results of the energy and frequency reconstruction. The predicted energy error for  $^{120}\text{Sn}$  over all events is normally distributed with a standard deviation of 2.3 eV (a). This corresponds to an event-by-event reconstructed rest frame transition frequency with an error around 2 MHz when 100 target atoms events are detected, which is further decreased to only 2.5 kHz for  $10^8$  events (b). For  $^8\text{B}$ , an energy spread of 0.4 eV is obtained (c), corresponding to an uncertainty on the rest frame transition frequency of  $\sim 1.2$  MHz for  $10^4$  events (d). For  $^{48}\text{Ni}$ , the energy uncertainty is reduced to 77 eV (e), leading to a reconstructed rest frame transition frequency uncertainty at the MHz level, for  $10^6$  events (f).

by  $v_{\text{pred}} = \sum_i^N \frac{v_i}{dv_i^2} / \sum_i^N \frac{1}{dv_i^2}$  and its associated uncertainty:

$dv_{\text{pred}} = 1 / \sum_i^N \frac{1}{dv_i^2}$ , where  $v_i$  and  $dv_i$  are the predicted frequency and uncertainty, respectively, for the  $i$ th target atom event. In Fig. 3, we show the error in the calculated frequency as a function of the number of target atom events for the considered isotopes. For  $^{120}\text{Sn}$ , we can correctly predict the true value of the rest-frame transition frequency with an uncertainty of about 2 MHz with as little as 100 events and reach a precision at the 1 kHz level when  $10^8$  events of the target atom are measured. For  $^8\text{B}$ ,  $10^4$  events are needed to reach an uncertainty of  $\sim 1$  MHz on the measured transitions. This will allow the extraction of the charge radius of  $^8\text{B}$  with 10% relative uncertainty [28,57]. Finally, for  $^{48}\text{Ni}$ , an uncertainty of  $\sim 100$  MHz can be achieved for only  $10^2$  events. This level of precision will be enough for the extraction of the charge radius of  $^{48}\text{Ni}$  with 10% relative uncertainty [2,60]. We emphasize that performing spectroscopic measurements on light elements, such as boron, is challenging and currently impossible for  $^8\text{B}$  [28], while studying very short lived isotopes, such as  $^{48}\text{Ni}$  is completely out of the reach using available experimental techniques [14,20,44].

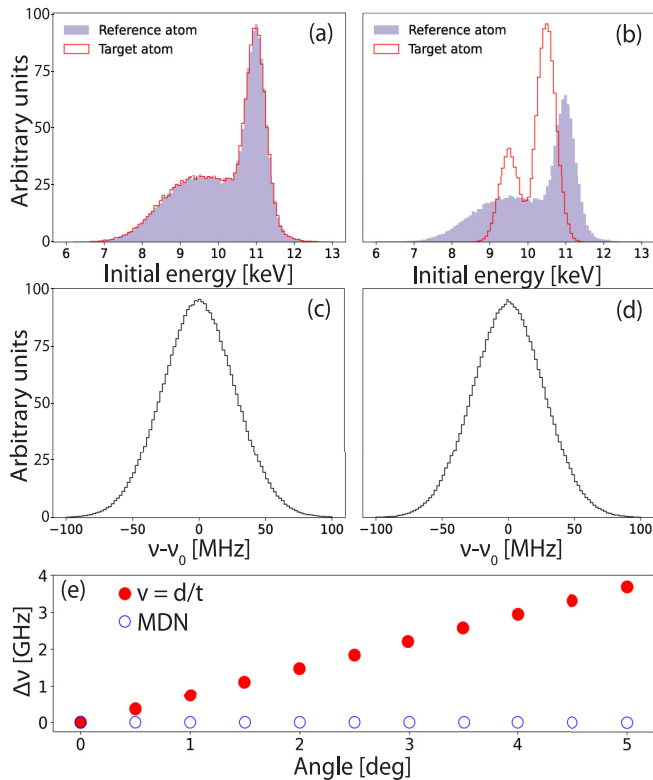


FIG. 4. Results of the frequency extraction for ions with non-Gaussian distributed initial energies for the  $^{120}\text{Sn}$  case. The energy histograms when the reference and target atom having the same and different initial energy distributions are shown in (a) and (b), while the associated reconstructed rest-frame frequency of the target atom using our proposed method, relative to the true rest-frame frequency,  $\nu_0$ , is shown in (c) and (d). (e) Difference,  $\Delta\nu$ , between true and reconstructed frequency, when using an MDN (blue circles) and when inferred from the distance and time information of the target atom only (red filled circles). The results are shown for different tilt angles of one electrode plate relative to the other (see main text for details).

To further explore the robustness of our approach in the case where the initial energy is not symmetrically distributed, we performed simulations assuming an arbitrary energy distribution, as shown in Fig. 4(a). This is particularly interesting as it indicates that our proposed scheme can be applied universally, for atoms and/or ions produced by diverse physical processes. For such a situation, simply applying a regular Doppler shift to the entire atomic ensemble, assuming a fixed acceleration voltage, would lead to distorted line shapes and add significant systematic uncertainties to the value of the extracted transition. However, as our method can recover the energy and hence the rest-frame frequency of individual atoms, using only the recorded parameters, it allows the scheme to be independent of the original energy distribution and produce consistent results for arbitrary distributions. This is shown in Fig. 4(c) for the case of  $^{120}\text{Sn}$ , where the distribution of the reconstructed rest-frame transition frequency has a well-behaved shape, from which the correct value of the frequency can be extracted with uncertainties at the 100 kHz level, with only  $10^4$  events.

Finally, we explore the situation in which the reference and target atoms have different initial energy distributions [Fig. 4(b)]. This is of interest when the production mechanism is a particularly violent one, as is often the case at radioactive beam facilities. The results obtained in this case are shown in Fig. 4(d). Again, we can recover the correct rest-frame transition frequency with similar uncertainties as described above, using arbitrary distributions for the initial energy. Similar results are obtained for the cases of  $^8\text{B}$  and  $^{48}\text{Ni}$  atoms with initial energies on the order of  $\sim 1$  keV and  $\sim 100$  keV, respectively, being able to reconstruct the rest frame transition frequencies with uncertainties comparable to those displayed in Fig. 3.

To study possible systematic uncertainties, numerical simulations under the following experimental conditions were performed: (i) one of the plates was tilted with respect to the beam propagation direction at different angles between 0 and 5 degrees, (ii) both plates were simultaneously tilted with respect to the horizontal at angles between 0 and 2 degrees, (iii) up to 10% relative uncertainties on the voltage applied to the two plates as well as on the distance between the plates were assumed, (iv) up to 5 millimeters of uncertainty on the vertical location of the ionization was assumed, (v) up to 5 millimeters of uncertainty on the distance between the two position sensitive detectors was assumed, and (vi) an additional transverse energy component of up to 1 keV to the ions was introduced. These values are significantly larger than one would expect from a properly implemented experimental setup. However, these uncertainties do not have a significant effect on the energy reconstruction of events. This is expected, as described above, given that during training, the MDN is able to learn all these variations of the experimental parameters which are encoded in the trajectories of the reference atoms and account for them in the predictions of the energies of the target atom.

A simple reconstruction of the target atom's velocity, taken as the ratio between the traveled distance and the time of flight, would be sensitive to the above-mentioned systematic uncertainties, leading to a wrong value of the rest frame transition frequency of the atom. The result of this approach is illustrated in Fig. 4(e), where the error in the reconstructed frequency is shown for different tilt angles between the two electrode plates. It can be seen that the shift in the reconstructed frequency is on the order of a few GHz with respect to the true rest-frame frequency (red filled circles). Moreover, this shift can't be reduced by increasing the accumulated statistics, thus being a limiting factor in extracting the physics of interest for most experiments. Additional experimental unknowns, such as an uncertainty in the distance between the two position-sensitive detectors, can lead to errors of similar magnitude, with  $\sim 1$  GHz frequency shifts for an uncertainty of two millimeters. On the other hand, it can be seen in Fig. 4(e) that the use of an MDN is largely insensitive to such experimental uncertainties (blue circles).

The main conditions that need to be fulfilled for the energy reconstruction to be successful with our proposed method are (i) the parameter space of the target atom needs to be contained within the parameter space of the reference one and (ii) enough events need to be recorded during the reference atom measurement for any region of interest in the parameter space. The first condition should be fulfilled by the geometric

constraints of the setup, i.e., the electron and ion should hit the position-sensitive detector for both ions. Moreover, one can easily compare the spatial and temporal information of the two species and confirm the validity of this assumption. The second condition depends only on the statistics accumulated while measuring the reference atom, which can be easily increased by several orders of magnitude if needed.

#### IV. CONCLUSION

We proposed a simple, versatile, and powerful experimental technique, suitable for performing high-resolution spectroscopy on fast, hot, short-lived isotopes produced with arbitrary energy distributions and large energy spreads. Using the temporal and spatial information of ions and corresponding electrons produced in a laser ionization process, the atoms' initial vector velocity can be reconstructed on an event-by-event basis, enabling precision measurements of the rest-frame transition frequency of the species of interest.

The described method is very efficient in terms of computing time, as the MDN needs to be trained initially, only once for a given energy range, using a reference atom. After that, predictions can be made for any other atom and transitions of interest. By increasing the number of events for the atom of interest,  $N_r$ , the uncertainty on the measured transition frequency, which scales as  $\frac{1}{\sqrt{N_r}}$ , can be further reduced. This can also be achieved by using detectors with better spatial and temporal resolutions compared to the ones considered here. Possible NN prediction biases can be estimated using the validation data set of the reference atom. The MDN predictions could potentially be further improved by using different learning rate schedules or trying more complex architectures

(in terms of layers, nodes per layers, or number of Gaussian components), compared to the one presented in this paper. The performance of other types of NN, able to estimate uncertainties for the predicted results, such as Bayesian NN [68], can also be investigated. Non-NN based methods could also offer a possible pathway for estimating the energies of interest. For example, for each target event, the energy and the associated uncertainty could be estimated in terms of the mean and standard deviation of the energy of the closest reference events in parameter space, where the number of such events would be optimized using the validation data.

The ability to perform precision measurements on fast beams with large energy spreads opens the way to studying short-lived isotopes at the extreme of existence, with lifetimes on the order of milliseconds or less. Such species can already be produced at different radioactive beam facilities worldwide, but their laser spectroscopic investigation is currently impossible with the available techniques. The proposed approach also opens the possibility to study isomeric states with sub-millisecond lifetimes that can be produced in flight by nuclear reactions.

#### ACKNOWLEDGMENTS

The authors thank the discussions with S. G. Wilkins, C. S. Sumithrarachchi, P. Mueller, F. C. Pastrana Cruz, and M. Paula Montes. This work was supported by the Office of Nuclear Physics, U.S. Department of Energy, under Grants No. DE-SC0021176 and No. DE-SC0021179, and the Jarve Seed fund. D.A.T. thanks the Laboratory of Nuclear Science at MIT for their hospitality during the sabbatical year when this work was performed, and the Universidad Nacional de Colombia for support under Grants No. 51111 and No. 51119.

- 
- [1] G. Arrowsmith-Kron, M. Athanasakis-Kaklamanakis, M. Au, J. Ballof, R. Berger, A. Borschevsky, A. A. Breier, F. Buchinger, D. Budker, L. Caldwell *et al.*, Opportunities for fundamental physics research with radioactive molecules, [arXiv:2302.02165](https://arxiv.org/abs/2302.02165).
  - [2] X. F. Yang, S. J. Wang, S. G. Wilkins, and R. F. Garcia Ruiz, Laser spectroscopy for the study of exotic nuclei, *Prog. Part. Nucl. Phys.* **129**, 104005 (2023).
  - [3] M. Block, M. Laatiaoui, and S. Raeder, Recent progress in laser spectroscopy of the actinides, *Prog. Part. Nucl. Phys.* **116**, 103834 (2021).
  - [4] R. F. Garcia Ruiz, M. L. Bissell, K. Blaum, A. Ekström, N. Frömmgen, G. Hagen, M. Hammen, K. Hebeler, J. D. Holt, G. R. Jansen *et al.*, Unexpectedly large charge radii of neutron-rich calcium isotopes, *Nat. Phys.* **12**, 594 (2016).
  - [5] A. J. Miller, K. Minamisono, A. Klose, D. Garand, C. Kujawa, J. D. Lantis, Y. Liu, B. Maaß, P. F. Mantica, W. Nazarewicz *et al.*, Proton superfluidity and charge radii in proton-rich calcium isotopes, *Nat. Phys.* **15**, 432 (2019).
  - [6] C. Gorges, L. V. Rodríguez, D. L. Balabanski, M. L. Bissell, K. Blaum, B. Cheal, R. F. Garcia Ruiz, G. Georgiev, W. Gins, H. Heylen *et al.*, Laser spectroscopy of neutron-rich tin isotopes: A discontinuity in charge radii across the  $N=82$  shell closure, *Phys. Rev. Lett.* **122**, 192502 (2019).
  - [7] R. P. de Groote, J. Billowes, C. L. Binnersley, M. L. Bissell, T. E. Cocolios, T. Day Goodacre, G. J. Farooq-Smith, D. V. Fedorov, K. T. Flanagan, S. Franchoo *et al.*, Measurement and microscopic description of odd-even staggering of charge radii of exotic copper isotopes, *Nat. Phys.* **16**, 620 (2020).
  - [8] M. Reponen, R. P. de Groote, L. Al Ayoubi, O. Beliuskina, M. L. Bissell, P. Campbell, L. Cañete, B. Cheal, K. Chrysalidis, C. Delafosse *et al.*, Evidence of a sudden increase in the nuclear size of proton-rich silver-96, *Nat. Commun.* **12**, 4596 (2021).
  - [9] A. Koszorús, X. F. Yang, W. G. Jiang, S. J. Novario, S. W. Bai, J. Billowes, C. L. Binnersley, M. L. Bissell, T. E. Cocolios, B. S. Cooper *et al.*, Charge radii of exotic potassium isotopes challenge nuclear theory and the magic character of  $N=32$ , *Nat. Phys.* **17**, 439 (2021).
  - [10] A. R. Vernon, R. F. Garcia Ruiz, T. Miyagi, C. L. Binnersley, J. Billowes, M. L. Bissell, J. Bonnard, T. E. Cocolios, J. Dobaczewski, G. J. Farooq-Smith *et al.*, Nuclear moments of indium isotopes reveal abrupt change at magic number 82, *Nat. Commun.* **607**, 260 (2022).
  - [11] T. Manovitz, R. Shaniv, Y. Shapira, R. Ozeri, and N. Akerman, Precision measurement of atomic isotope shifts using a two-isotope entangled state, *Phys. Rev. Lett.* **123**, 203001 (2019).
  - [12] J. Hur, D. P. L. Aude Craik, I. Counts, E. Knyazev, L. Caldwell, C. Leung, S. Pandey, J. C. Berengut, A. Geddes, W. Nazarewicz



- et al.*, Evidence of two-source king plot nonlinearity in spectroscopic search for new boson, *Phys. Rev. Lett.* **128**, 163201 (2022).
- [13] R. Neugart, J. Billowes, M. L. Bissell, K. Blaum, B. Cheal, K. T. Flanagan, G. Neyens, W. Nörtershäuser, and D. T. Yordanov, Collinear laser spectroscopy at ISOLDE: New methods and highlights, *J. Phys. G: Nucl. Part. Phys.* **44**, 064002 (2017).
- [14] K. Minamisono, P. F. Mantica, A. Klose, S. Vinnikova, A. Schneider, B. Johnson, and B. R. Barquest, Commissioning of the collinear laser spectroscopy system in the BECOLA facility at NSCL, *Nucl. Instrum. Methods Phys. Res., Sect. A* **709**, 85 (2013).
- [15] R. F. Garcia Ruiz, R. Berger, J. Billowes, C. L. Binnersley, M. L. Bissell, A. A. Breier, A. J. Brinson, K. Chrysalidis, T. E. Cocolios, B. S. Cooper *et al.*, Spectroscopy of short-lived radioactive molecules, *Nature (London)* **581**, 396 (2020).
- [16] S. M. Udrescu, A. J. Brinson, R. F. Garcia Ruiz, K. Gaul, R. Berger, J. Billowes, C. L. Binnersley, M. L. Bissell, A. A. Breier, K. Chrysalidis *et al.*, Isotope shifts of radium monofluoride molecules, *Phys. Rev. Lett.* **127**, 033001 (2021).
- [17] S.-M. Udrescu, S. G. Wilkins, A. Breier, R. F. Garcia Ruiz, M. Athanasakis-Kaklamanakis, M. Au, I. Belosevic, R. Berger, M. Bissell, C. L. Binnersley *C et al.*, Precision spectroscopy and laser-cooling scheme of a radium-containing molecule, *Nat. Phys.* (2024).
- [18] S. G. Wilkins, S.-M. Udrescu, M. Athanasakis-Kaklamanakis, R. F. Garcia-Ruiz, M. Au, I. Belosevic, R. Berger, M. Bissell, A. A. Breier, A. J. Brinson *et al.*, Observation of the distribution of nuclear magnetization in a molecule, [arXiv:2311.04121](https://arxiv.org/abs/2311.04121) (2023).
- [19] T. Glasmacher, B. Sherrill, W. Nazarewicz, A. Gade, P. Mantica, J. Wei, G. Bollen, and B. Bull, Facility for rare isotope beams update for nuclear physics news, *Nucl. Phys. News* **27**, 28 (2017).
- [20] Y. Yano and T. Motobayashi, Radioactive Isotope Beam Factory at RIKEN (RIBF), *Nucl. Phys. News* **17**, 5 (2007).
- [21] R. F. Garcia Ruiz, A. R. Vernon, C. L. Binnersley, B. K. Sahoo, M. Bissell, J. Billowes, T. E. Cocolios, W. Gins, R. P. de Groot, K. T. Flanagan *et al.*, High-precision multiphoton ionization of accelerated laser-ablated species, *Phys. Rev. X* **8**, 041005 (2018).
- [22] J. Jovanović and R. F. Garcia Ruiz, Modeling of transient interference phenomena in colinear laser spectroscopy, *Phys. Rev. A* **107**, 013104 (2023).
- [23] D. R. Leibbrandt, S. G. Porsev, C. Cheung, and M. S. Safronova, Prospects of a thousand-ion  $\text{Sn}^{2+}$  Coulomb-crystal clock with sub- $10^{-19}$  inaccuracy, [arXiv:2205.15484](https://arxiv.org/abs/2205.15484).
- [24] D. T. Yordanov, L. V. Rodríguez, D. L. Balabanski, J. Bieroń, M. L. Bissell, K. Blaum, B. Cheal, J. Ekman, G. Gaigalas, R. F. Garcia Ruiz *et al.*, Structural trends in atomic nuclei from laser spectroscopy of tin, *Commun. Phys.* **3**, 107 (2020).
- [25] M. H. Smedberg, T. Baumann, T. Aumann, L. Axelsson, U. Bergmann, M. J. G. Borge, D. Cortina-Gil, L. M. Fraile, H. Geissel, L. Grigorenko *et al.*, New results on the halo structure of  $^8\text{B}$ , *Phys. Lett. B* **452**, 1 (1999).
- [26] G. A. Korolev, A. V. Dobrovolsky, A. G. Inglessi, G. D. Alkharov, P. Egelhof, A. Estradé, I. Dillmann, F. Farinon, H. Geissel, S. Ilieva *et al.*, Halo structure of  $^8\text{B}$  determined from intermediate energy proton elastic scattering in inverse kinematics, *Phys. Lett. B* **780**, 200 (2018).
- [27] A. V. Dobrovolsky, G. A. Korolev, A. G. Inglessi, G. D. Alkharov, G. Coló, I. Dillmann, P. Egelhof, A. Estradé, F. Farinon, H. Geissel *et al.*, Nuclear-matter distribution in the proton-rich nuclei  $^7\text{Be}$  and  $^8\text{B}$  from intermediate energy proton elastic scattering in inverse kinematics, *Nucl. Phys. A* **989**, 40 (2019).
- [28] Bernhard Maaß, Laser spectroscopy of the boron isotopic chain, Ph.D. thesis, Technische Universität Darmstadt, 2020.
- [29] J. N. Bahcall, F. H. Walter S. H. Lubow, P. D. Parker, and R. K. Ulrich, Standard solar models and the uncertainties in predicted capture rates of solar neutrinos, *Rev. Mod. Phys.* **54**, 767 (1982).
- [30] K. Riisager and A. S. Jensen, The radius of  $^8\text{B}$  and solar neutrinos, *Phys. Lett. B* **301**, 6 (1993).
- [31] B. Blank, M. Chartier, S. Czajkowski, J. Giovinazzo, M. S. Pravikoff, J.-C. Thomas, G. de France, F. de Oliveira Santos, M. Lewitowicz, C. Borcea *et al.*, Discovery of doubly magic  $^{48}\text{Ni}$ , *Phys. Rev. Lett.* **84**, 1116 (2000).
- [32] L. V. Grigorenko, R. C. Johnson, I. G. Mukha, I. J. Thompson, and M. V. Zhukov, Theory of two-proton radioactivity with application to  $^{19}\text{Mg}$  and  $^{48}\text{Ni}$ , *Phys. Rev. Lett.* **85**, 22 (2000).
- [33] S. V. Pineda, K. König, D. M. Rossi, B. A. Brown, A. Incorvati, J. Lantis, K. Minamisono, W. Nörtershäuser, J. Piekarewicz, R. Powel *et al.*, Charge radius of neutron-deficient  $^{54}\text{Ni}$  and symmetry energy constraints using the difference in mirror pair charge radii, *Phys. Rev. Lett.* **127**, 182503 (2021).
- [34] W. Demtröder, *Laser Spectroscopy 2: Experimental Techniques* (Springer, New York, 2015).
- [35] H. Carstens, S. Holzberger, J. Kaster, J. Weitenberg, V. Pervak, A. Apolonski, E. Fill, F. Krausz, and I. Pupeza, Large-mode enhancement cavities, *Opt. Express* **21**, 11606 (2013).
- [36] A. R. Vernon, J. Billowes, C. L. Binnersley, M. L. Bissell, T. E. Cocolios, G. J. Farooq-Smith, K. T. Flanagan, R. F. Garcia Ruiz, W. Gins, R. P. de Groot *et al.*, Simulation of the relative atomic populations of elements  $1 \leq Z \leq 89$  following charge exchange tested with collinear resonance ionization spectroscopy of indium, *Spectrochim. Acta, Part B* **153**, 61 (2019).
- [37] F. P. Gustafsson, C. M. Ricketts, M. L. Reitsma, R. F. Garcia Ruiz, S. W. Bai, J. C. Berengut, J. Billowes, C. L. Binnersley, A. Borschevsky, T. E. Cocolios *et al.*, Tin resonance-ionization schemes for atomic- and nuclear-structure studies, *Phys. Rev. A* **102**, 052812 (2020).
- [38] A. P. Galván *et al.*, Status update on the  $\beta$ - $\nu$  Correlation Measurement in the  $\beta$  Decay of  $^8\text{B}$ , in *Proceedings of the Conference on Advances in Radioactive Isotope Science (ARIS2014)* (Tokyo, Japan, 2015), p. 030071.
- [39] J. Dilling, R. Krücken, and G. Ball, ISAC overview, *Hyperfine Interact.* **225**, 1 (2014).
- [40] I. D. Moore, P. Dendooven, and J. Ärje, *The IGISOL technique—three decades of developments*, Three decades of research using IGISOL technique at the University of Jyväskylä A Portrait of the Ion Guide Isotope Separator On-Line Facility in Jyväskylä (Berlin, Germany, 2014), pp. 15–60.
- [41] M. J. Borge and B. Jonson, ISOLDE past, present and future, *J. Phys. G: Nucl. Part. Phys.* **44**, 044011 (2017).
- [42] R. Kallenbach, M. Gonin, P. Bochsler, and A. Bürgi, Charge exchange of B, C, O, Al, Si, S, F and Cl passing through thin carbon foils at low energies: Formation of negative ions, *Nucl. Instrum. Methods Phys. Res., Sect. B* **103**, 111 (1995).

- [43] J. M. Brown and A. Carrington, *Rotational Spectroscopy of Diatomic Molecules* (Cambridge University Press, Cambridge, 2003).
- [44] K. Cooper, C. S. Sumithrarachchi, D. J. Morrissey, A. Levand, J. A. Rodriguez, G. Savard, S. Schwarz, and B. Zabransky, Extraction of thermalized projectile fragments from a large volume gas cell, *Nucl. Instrum. Methods Phys. Res., Sect. A* **763**, 543 (2014).
- [45] C. Sumithrarachchi (private communication).
- [46] T. Schenkel, M. A. Briere, H. Schmidt-Böcking, K. Bethge, and D. H. Schneider, Electronic sputtering of thin conductors by neutralization of slow highly charged ions, *Phys. Rev. Lett.* **78**, 2481 (1997).
- [47] T. Schenkel, A. V. Hamza, A. V. Barnes, and D. H. Schneider, Interaction of slow, very highly charged ions with surfaces, *Prog. Surf. Sci.* **61**, 23 (1999).
- [48] R. A. Wilhelm, E. Gruber, J. Schweska, R. Heller, S. Fascko, and F. Aumayr, Neutralization dynamics of slow highly charged ions in 2D materials, *Appl. Sci.* **8**, 1050 (2018).
- [49] R. Dörner, V. Mergel, O. Jagutzki, L. Spielberger, J. Ullrich, R. Moshhammer, and H. Schmidt-Böcking, Cold target recoil ion momentum spectroscopy: A ‘momentum microscope’ to view atomic collision dynamics, *Phys. Rep.* **330**, 95 (2000).
- [50] J. Ullrich, R. Moshhammer, A. Dorn, R. Dörner, L. P. H. Schmidt, and H. Schmidt-Böcking, Recoil-ion and electron momentum spectroscopy: Reaction-microscopes, *Rep. Prog. Phys.* **66**, 1463 (2003).
- [51] W. Jiang, X. Wang, S. Zhang, R. Dong, Y. Guo, J. Feng, Z. Shen, Z. Zhu, and Y. Jiang, A reaction microscope for AMO science at Shanghai soft X-ray free-electron laser facility, *Appl. Sci.* **12**, 1821 (2022).
- [52] X. Gong, P. He, Q. Song, Q. Ji, H. Pan, J. Ding, F. He, H. Zeng, and J. Wu, Two-dimensional directional proton emission in dissociative ionization of H<sub>2</sub>, *Phys. Rev. Lett.* **113**, 203001 (2014).
- [53] U. S. Sainadh, H. Xu, X. Wang, A. Atia-Tul-Noor, W. C. Wallace, N. Douguet, A. Bray, I. Ivanov, K. Bartschat, A. Kheifets *et al.*, Attosecond angular streaking and tunnelling time in atomic hydrogen, *Nature (London)* **568**, 75 (2019).
- [54] A. Lurio, R. L. de Zafra, and R. J. Goshen, Lifetime of the first <sup>1</sup>P<sub>1</sub> state of zinc, calcium, and strontium, *Phys. Rev.* **134**, A1198 (1964).
- [55] R. Engleman and E. S. Chang, High-resolution spectroscopy of Ca, Sr and Ba hollow cathodes, in *Fourier Transform Spectroscopy* (Optica Publishing Group, Washington DC, 1999).
- [56] C. M. Bishop, Mixture density networks, *Neural Computing Research Group, Aston University*, Technical Report NCRG/94/004, 1994.
- [57] B. Maaß, T. Hüther, K. König, J. Krämer, J. Krause, A. Lovato, P. Müller, K. Pachucki, M. Puchalski, R. Roth *et al.*, Nuclear charge radii of <sup>10,11</sup>B, *Phys. Rev. Lett.* **122**, 182501 (2019).
- [58] M. C. E. Huber and R. J. Sandeman, Oscillator strengths of ultraviolet NI I lines from hook-method and absorption measurements in a furnace, *Astron. Astrophys.* **86**, 95 (1980).
- [59] L. V. Rodríguez, D. L. Balabanski, M. L. Bissell, K. Blaum, B. Cheal, G. De Gregorio, J. Ekman, R. F. Garcia Ruiz, A. Gargano, G. Georgiev *et al.*, Doubly-magic character of <sup>132</sup>Sn studied via electromagnetic moments of <sup>133</sup>Sn, *Phys. Rev. C* **102**, 051301(R) (2020).
- [60] S. Malbrunot-Ettenauer, S. Kaufmann, S. Bacca, C. Barbieri, J. Billowes, M. L. Bissell, K. Blaum, B. Cheal, T. Duguet, R. F. Garcia Ruiz *et al.*, Nuclear charge radii of the nickel isotopes <sup>58–68,70</sup>Ni, *Phys. Rev. Lett.* **128**, 022502 (2022).
- [61] J. Tanaka, Z. Yang, S. Typel, S. Adachi, S. Bai, P. van Beek, D. Beaumel, Y. Fujikawa, J. Han, S. Heil *et al.*, Formation of  $\alpha$  clusters in dilute neutron-rich matter, *Science* **371**, 260 (2021).
- [62] P.-G. Reinhard, W. Nazarewicz, and R. F. Garcia Ruiz, Beyond the charge radius: The information content of the fourth radial moment, *Phys. Rev. C* **101**, 021301(R) (2020).
- [63] R. A. Müller, V. A. Yerokhin, A. N. Artemyev, and A. Surzhykov, Nonlinearities of King’s plot and their dependence on nuclear radii, *Phys. Rev. A* **104**, L020802 (2021).
- [64] D. A. Dahl, SIMION 3D Version 7.0, computer program, Idaho National Engineering and Environmental Laboratory.
- [65] A. Paszke, S. Gross, F. Massa, A. Lerer, J. Bradbury, G. Chanan, T. Killeen, Z. Lin, N. Gimelshein, L. Antiga *et al.*, PyTorch: An imperative style, high-performance deep learning library, in *Advances in Neural Information Processing Systems*, 32 ed. (Curran Associates, Inc., 2019), pp. 8024–8035.
- [66] A. B. Guillaumes, Mixture density networks for distribution and uncertainty estimation, Ph.D. thesis, Universitat Politècnica de Catalunya. Facultat d’Informàtica de Barcelona, 2017.
- [67] D. P. Kingma and J. Ba, Adam: A method for stochastic optimization, [arXiv:1412.6980](https://arxiv.org/abs/1412.6980).
- [68] R. M. Neal, *Bayesian Learning for Neural Networks* (Springer Science & Business Media, 2012), Vol. 118.